Large-Scale Nano Piezo Force Position Arrays as Ultrahigh-Resolution Micro- and Nanoparticle Tracker

Kittitat Subannajui, Andreas Menzel,* Firat Güder, Yang Yang, Katrin Schumann, Xiaoli Lu, and Margit Zacharias**

Defining the position of an object on a planar substrate by force sensors is a common technology nowadays. Many products are commercialized worldwide, which make use of force sensors, especially, for instance, touchpads. Here advanced lithography processes together with piezoelectric materials are demonstrated to fabricate an extremely high resolution force sensor. The approach combines a large array of nanoscale piezoelectric lines fabricated on Si wafer by phase-shift lithography and atomic-layer-deposition-based spacer lithography techniques. These key lithography methods are utilized to fabricate ultralong (cm range) nanolines on the wafer scale. ZnO and P(VDF-TrFE) are selected here as materials for piezoelectric signal generators. The detection mechanisms are explained and simulations combined with experimental data are demonstrated to prove the concept. The signal generated when an object approaches one single line is in the nanoampere range. The result enables a new and simple path for a device fabrication, which defines the position with micro- and nanometer resolution and can be used, for example, as micro- and nanoparticle trackers.

Dr. K. Subannajui, A. Menzel, Dr. F. Güder,
Dr. Y. Yang, Prof. M. Zacharias
Laboratory for Nanotechnology
Department of Microsystems Engineering (IMTEK)
University of Freiburg
Freiburg 79110, Germany
E-mail: kchantavong@hotmail.com;
andreas.menzel@imtek.uni-freiburg.de;
zacharias@imtek.de

K. Subannajui
Faculty of Science
Mahidol University
272 Rama VI Road, Ratchathewi District, Bangkok 10400, Thailand

K. Schumann
Institute for Applied Materials
Karlsruhe Insitute of Technology (KIT)
D-76344 Eggenstein-Leopoldshafen, Germany

Dr. X. Lu
State Key Discipline Laboratory of Wide Band Gap Semiconductor Technology
School of Microelectronics
Xidian University
Xi'an 710071, China

Prof. M. Zacharias
FRIAS, School of Soft Matter Research
University of Freiburg
Albertstraße 19, 79104 Freiburg, Germany

DOI: 10.1002/adfm.201201201

1. Introduction

Touchpads can be categorized based on the principle used, for example, resistive, capacitive, piezoelectric, surface acoustic wave, or optical imaging. Among those found in the market, the capacitive-based touchpad is the most favorable in terms of finger-based operation. The accuracy of a defined position is good enough for personal computers or portable-device applications. However, most of the devices mentioned above are still in the early state of technology, which is yet to be fully developed. Even though current force-sensor technologies are available and used in industrial applications, such a technology is still not suitable for extreme scientific requirements, for example, a rapid spatial detection of micro- or nanosized objects. In order to obtain a device with such a superior space-selective performance, a new fabrication concept is needed. The piezoelectric effect is a very promising property which can be implemented to enhance the performance of touchpad sensors. Currently, piezoelectric materials are widely used in many precision-controlled instruments. The piezoelectric property allows the conversion between the mechanical force and the electrical signal and is applied in many scientific devices for example, piezomotors in robot arms and atomic force microscopy (AFM) tips, light sparkers, quartz oscillators for transmitters and receivers, and other kinds of piezoactuators.[1–5] With the advance of nanotechnology, the dimension of piezoelectric materials can be significantly reduced. Apparently, when the size of the material is reduced, the piezoelectric effect is still properly functional.[6,7] This piezoelectric nanomaterial can be single-crystalline or polycrystalline both of which were reported to yield a reliable piezoelectric response.[8,9] Conventional lithography is incapable of producing nanostructures. On the other hand, high-resolution lithography processes like electron-beam lithography (e-beam lithography) are limited by the size of the exposed lithographic area. Furthermore, the e-beam lithography process is not suitable for mass-production due to time consumption and the stability of the e-beam. In this paper, we aim to improve the resolution of a force-sensor array and its performance by implementing piezoelectric materials into novel advanced fabrication processes. We propose the use of phase-shift lithography (PSL) and atomic-layer-deposition (ALD)-based spacer

lithography (ASL) for sensor-array fabrication with extremely high resolution.

2. Results and Discussion

Phase-shift lithography is one of the most flexible lithographic methods for nanostructure fabrication. The physical principle of this method is to manipulate the destructive interference of light through a transparent mask (for example on an inexpensive borosilicate mask). The resolution of PSL scales down from 300 nm to below 100 nm, which is small enough for our application. In a similar manner to PSL techniques, interference-lithography-based maskless techniques (e.g., laser interference lithography) are also capable of fabricating ordered line patterns in these dimensions. PSL offers big advantages in terms of precision on 4 inch wafers or even larger ones, which allows an additional alignment for complex nanostructures.[10,11] The PSL mask is fabricated by a normal photolithography layout and the design is composed of step lines of 1 μm separation and 1 cm length, with a depth adjusted to the desired interference enhancement. In **Figure 1**a, the fabrication process starts by choosing a desired non-conductive substrate which is Al_2O_3/Si in our case (Step I). A polycrystalline 100 nm-thick piezoelectric ZnO layer was deposited by ALD at 150 °C (Step II). The low temperature ALD ZnO and Al_2O_3 thin-film growth we used is described elsewhere.[12] For the lithography steps, we use an image reversal photoresist AZ 5214e without a reversal bake and flood exposure, such that the AZ 5214e was used as a positive resist (Step III). The phase-shift-lithography mask was placed on the top of the photoresist and UV light was exposed on the wafer (Step IV). After exposure, the sample was developed in AZ 726 MIF developer, and the photoresist was dissolved, except at the dark interference areas (Step V). Photoresist nanolines appeared on the ZnO surface. By using the obtained photoresist nanolines as an etching mask, ZnO was etched away by a CF_4/CHF_3/Ar-based reactive ion etching (RIE) process (Step VI). Note that the underlying Al_2O_3 layer serves as an etch stop layer during the RIE process. This etched stop layer can minimize the damage of the plasma due to the selective etching of CF_4/CHF_3/Ar-based RIE. After removing the remnant resist nanolines by O_2 plasma, the piezoelectric ZnO nanolines are obtained (Step VII). These piezoelectric ZnO lines are depicted in Figure 1d. If a thin dielectric layer is deposited (which can be a homogeneous deposited Al_2O_3 layer by ALD) over the piezoelectric lines, a second array of lines can be fabricated by 90° rotation in the same manner. Once the dielectric layer is etched anisotropically, all of the piezoelectric lines are exposed to the surface. Afterwards, the piezoelectric lines were coated by a protective layer to prevent the sensing lines from suffering mechanical damage. We have named this first type of force-sensor array the PSL sensor.

The second type of sensor array was fabricated by employing ALD spacer lithography (ASL). Spacer lithography is a very reliable method of fabricating a nanoscale high-aspect-ratio structure on any desired position of a substrate. The size of

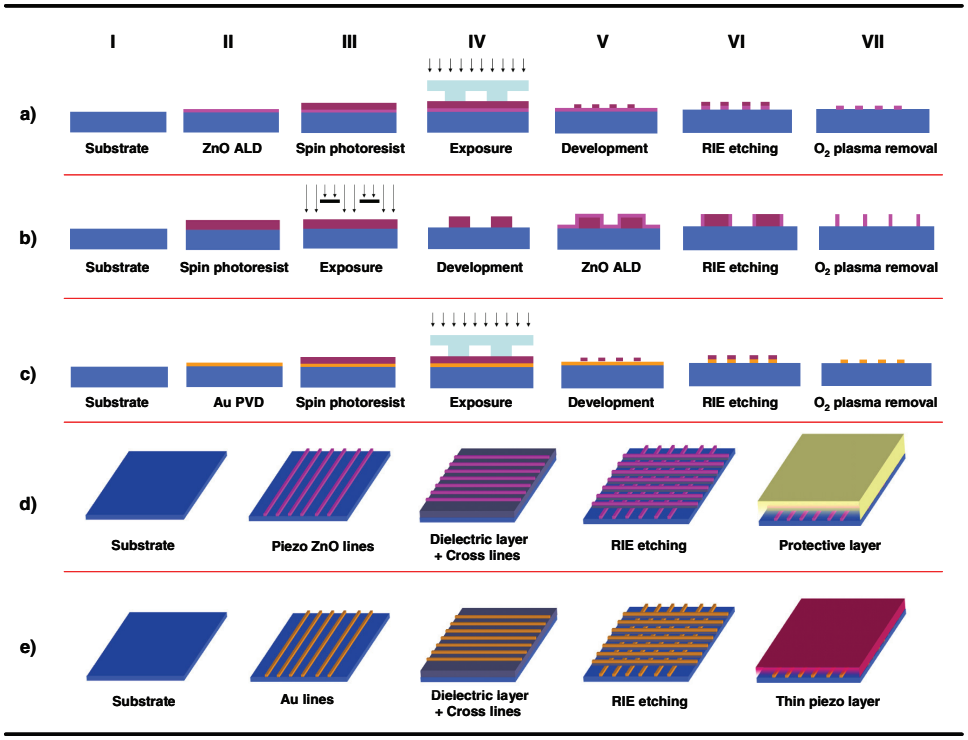

Figure 1. Advanced lithographic fabrication processes for high-resolution force position detectors. a–c) Fabrication of nanolines on the wafer scale for devices based on PSL (a), ASL (b), and P(VDF-TrFE) (c). d) Demonstration of how to obtain the fabrication 2D resolution of ZnO lines for PSL and ASL devices. e) Fabrication of 2D-resolution devices based on P(VDF-TrFE) polymer.

the nanostructure can be controlled by the film deposition thickness which can vary from thicker than 100 nm to less than 10 nm.[13,14] In Figure 1b, the ASL method starts by spin-coating of AZ 701 MIR photoresist (Step II) and normal exposure through a microstructured chrome mask (Step III). After developing, parallel arranged photoresist blocks with vertical sidewalls were obtained (Step IV). Then, an ALD ZnO film with the thickness of 100 nm was deposited homogeneously on the photoresist and substrate (Step V). Afterwards, the 100 nm ZnO film was etched anisotropically by RIE (Step VI). O_2 plasma was used to burn the remnant photoresist blocks away. As a result, remaining ZnO walls with a height equal to the original photoresist thickness were obtained. The cross lines and the protective layer can be fabricated in the same way as explained in PSL sensors in Figure 1d. This second type of force-sensor arrays fabricated by ASL will be called the ASL sensor. A photograph of the full wafer including the metal connection lines is shown as an example in Figure S1 (Supporting Information).

The last type of force position detectors presented in this work is based on a piezoelectric polymer film, poly(vinylidene fluoride trifluoroethylene) (P(VDF-TrFE)). P(VDF-TrFE) is a polymer that exhibits excellent piezoelectric properties. The piezoelectric phenomenon in polymer occurs due to the change of the dipole density with respect to the applied mechanical stimulus. The piezoelectric coefficient of P(VDF-TrFE) is in the same order to that of piezoelectric ceramics which implies a high performance in electromechanical conversion.[15,16] Our fabrication scheme of the third force position detection array starts with Au lines structured by phase-shift lithography (Figure 1c). The fabrication method is almost identical to the PSL sensor mentioned above, except that the ALD ZnO film was substituted by an evaporated Au film of 100 nm. As a result of the respective PSL process Au lines are established as shown in Figure 1e. The cross Au line array was produced on a dielectric layer on top of the first Au line array and physically etched away to expose the structure. At the end, a thin P(VDF-TrFE) film was homogeneously deposited on the Au nanolines and annealed at 135 °C for 2 minutes. This type of force-sensor array will be called the P(VDF-TrFE) sensor from now on.

Depending on the nanostructure geometry and crystallography, the performance of all three piezoelectric force sensors can be different. **Figure 2**–c show high-resolution scanning electron microscopy (HRSEM) images of the fabricated PSL, ASL, and P(VDF-TrFE) sensors, respectively. In Figure 2a, the geometry of PSL sensors in terms of thickness × width × length was 100 nm × 300 nm × 10 mm. If the force-interacting volume of the piezoelectric line is reduced, then the generated signal will decrease. Therefore, the width of the PSL ZnO lines was kept at 300 nm; even though smaller widths of the PSL ZnO lines can be easily achieved with the method presented here. In Figure 2b, the geometry of the ASL sensor was chosen as 1000 nm × 100 nm × 10 mm. The 1000 nm thickness of the ASL ZnO lines was equal to the photoresist thickness and the shape of ASL ZnO lines is identical to ZnO nanowalls with an extremely high aspect ratio. A large volume can be conserved while the line width is gradually reduced. Hence, the ASL technique reported here provides the opportunity of achieving a much higher resolution force-sensor array in the future. In Figure 2c, Au lines with the width of 150–170 nm were observed. These Au lines operate as electrodes to trap the charge carriers generated by the P(VDF-TrFE) film.

The crystallography of piezoelectric ZnO and P(VDF-TrFE) can be observed from X-ray diffraction (XRD) patterns. In Figure 2d, the SEM images reveal the free-standing cross sections of ASL nanowalls. The wall-like structure has the advantage in that the size of nanostructure can be much smaller while the mass of lines is still large. These free-standing ASL nanowalls including the PSL nanolines conserve the high-quality polycrystallinity of the ZnO nanofilms obtained from ALD. This high crystallinity is a very important factor which has to be preserved in order to obtain an electrical signal stimulated by an external applied force from the ZnO nanolines. In Figure 2e, the P(VDF-TrFE) structure was observed by HRSEM. The structure composes of several circular shape structures which imply crystallization of the polymer. XRD results were used to investigate the crystallization of the ZnO ALD layer and the P(VDF-TrFE) polymer. Apparently, the preferential orientation of a thin ZnO film (30 nm) is a single peak at around 32.5° which could be a shift of a ZnO orientation (Figure 2f), while the (002) orientation becomes stronger if the film is getting thicker (100 nm) (Figure 2g). The pre-deposited Al_2O_3 layer in this study is amorphous in nature and, therefore, a related peak in the XRD pattern cannot be identified.[17] The XRD results from the P(VDF-TrFE) polymer show a strong peak at 20°, which implies that the β-phase is dominant in the polymer film. Out of several possible phases, the β-phase is the only piezoelectric phase in P(VDF-TrFE).

The three sensor arrays operate with the same functionality as explained in **Figure 3**a. If a stimulus force acts on the surface, an electrical signal is generated in both the x and y directions. Because the two separated lines are disconnected from each other, once the signal is realized in a specific line, the position can be identified. The mechanism of electrical signal generation can be divided into two methods. The first method is according to a generated signal due to a direct mechanical stimulus on a piezoelectric line as shown in Figure 3b. The electrical signal in PSL sensors and ASL sensors can be explained by this principle. The nanolines in ASL and PSL sensors must be able to generate and conduct electricity at the same time. In consequence, ZnO lines have to be sufficient large enough to attain a low resistance and a high piezoelectric volume. For the second method, the electrical signal is generated in the piezoelectric polymer film corresponding to the applied force. The charge carriers in the film are trapped by the biased Au electrode and the signal is detected as shown in Figure 3c. Due to a very low conductivity of the polymer, the Au line with the highest signal is the one closest to the mechanical stimulus position. The electrical signal in P(VDF-TrFE) is also derived from the same principle as this method.

Since the resolution of piezoelectric position detectors can be controlled by adjusting the line dimension and gaps, PSL and ASL become convenient lithography methods to accomplish such high-resolution piezoelectric force-sensor arrays. A schematic of such an arrangement is shown in Figure 3a and the position (x, y) of an object or a tip/particle can be analyzed. The resolution of this realized device is much higher than a typical touchpad in the market to date.

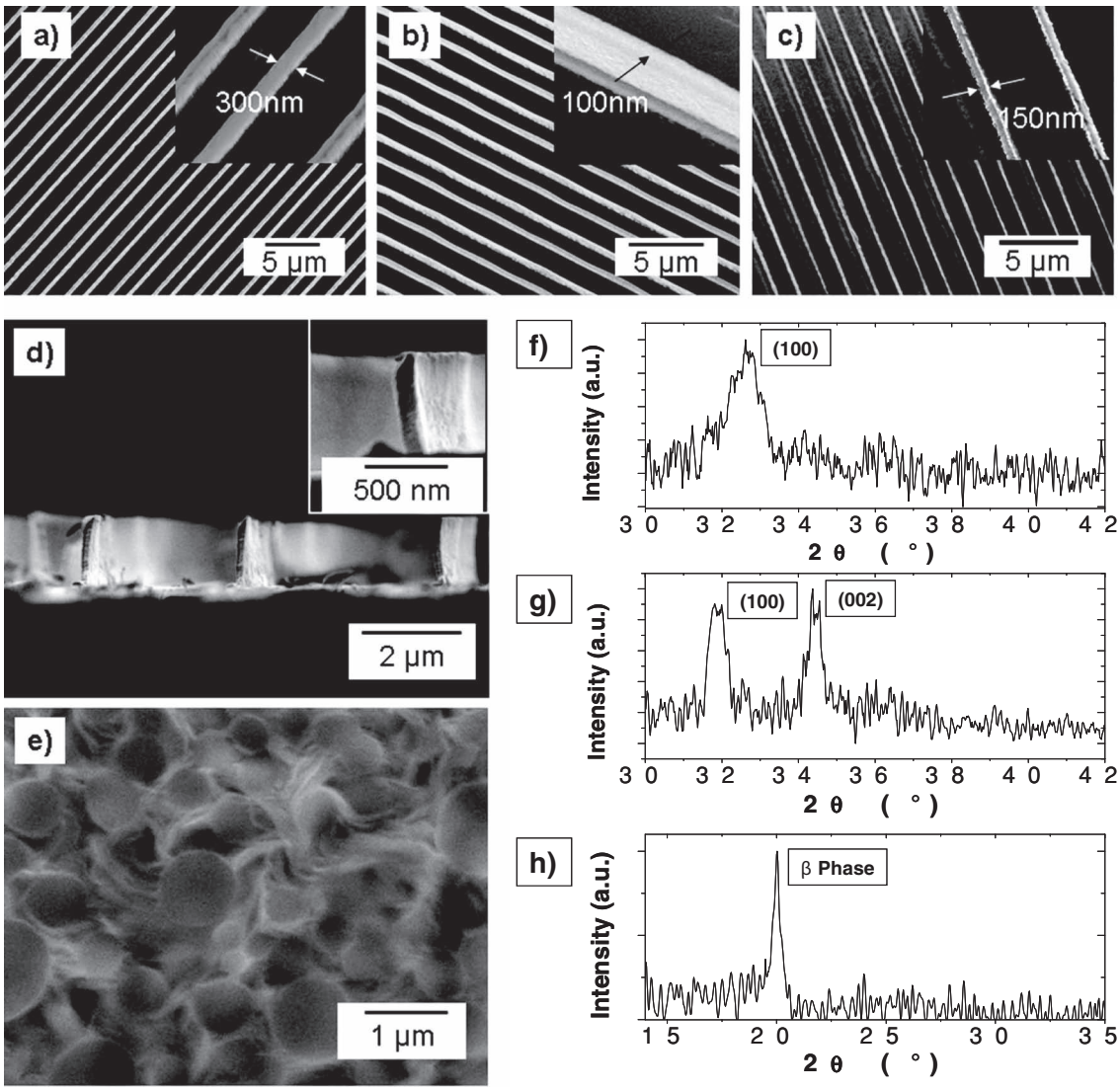

Figure 2. a–c) HRSEM images of ZnO PSL (a), ASL (b) and Au (c) PSL nanolines on Al_2O_3 on Si substrates. d) HRSEM images of the polycrystalline ZnO deposited film by ALD. e) HRSEM image of the P(VDF-TrFE) polymer and its grains. f,g) X-ray diffraction pattern (XRD) of ZnO film by ALD. h) XRD data of P(VDF-TrFE) films.

Piezoelectricity of ZnO is the result of the large anisotropic property of Zn^{2+} cation and O^{2-} anion. In a single-crystal material, the piezoelectric coefficients are varied with the crystal directions. Under an applied stress, the atomic displacement occurring in the crystal causes a dipole moment in the lattice, and the add-up effect finally induces a potential difference in the material. Therefore, the piezoelectricity is in principle another orientation-dependent material property. On the other hand, according to a study by Damjanovic, the centrosymmetric property of polycrystalline non-ferroelectric material is normally incapable of maintaining piezoelectricity.[18] A formation of "completely random oriented" grains eliminates a piezoelectricity in polycrystalline ZnO. However, in many typical ZnO fabrications, the polycrystalline ZnO usually contains a preferred orientation, especially in thin film structures.[19] Kim et al.[20] reported a force-sensor device based on ZnO thin films (ALD ZnO/Al_2O_3/Si). The grain size at the interface between the ZnO and Al_2O_3 is small and random oriented, but the further away the grains are, the larger the (001) preferential orientation. A detailed study of piezoelectricity of polycrystalline ZnO thin film was carried out by Bdikin et al.[21] Although the piezoelectricity in polycrystalline is weaker, unipolarity in polycrystalline still exists. In Figure 2f,g, the XRD results confirm that the effects occur in our ALD films quite clearly. Hence, the piezoelectricity of our ZnO thin film is preserved, though weaker than that of the single-crystalline ZnO. We have now implemented the necessary piezoelectric properties of ZnO for the physical characterization of a force detection device in a finite-element simulation. By using strain-charge coupled equations as a constructive piezoelectric calculation, the simulation result of a PSL piezoelectric line is shown in Figure 3d. In our simulation, the applied force is assumed to be a point force of 1 μN. The electrical field distribution over a symmetric structure is composed of both positive and negative fields

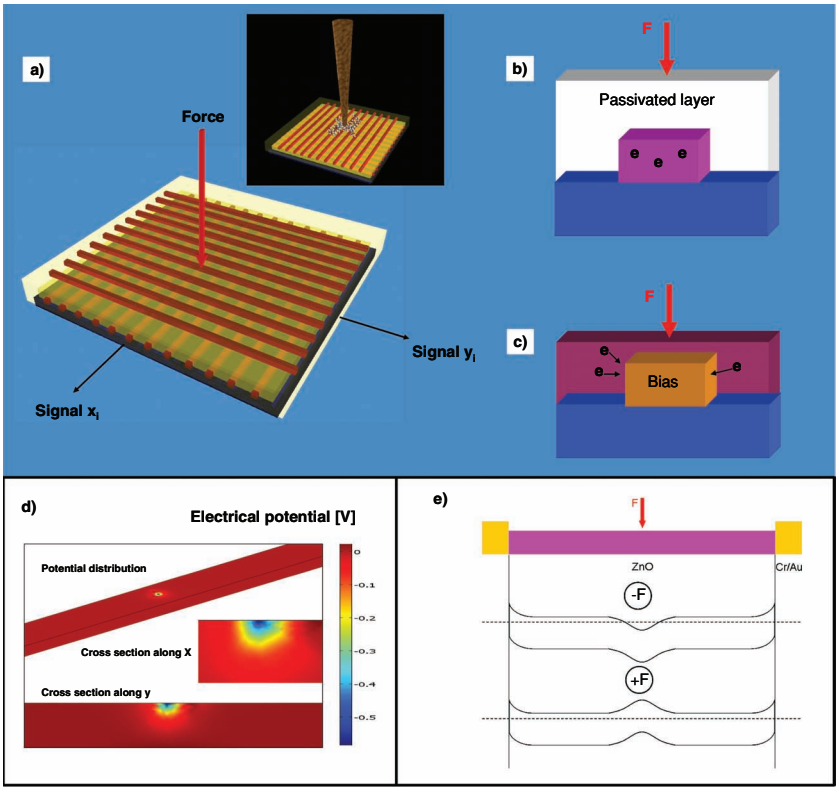

Figure 3. a) Schematics of nano piezo touchpad. Functional lines (ZnO or Au) are crossed and separated by a dielectric layer. The crossed lines are fabricated on an Al_2O_3-covered Si substrate. b) Cross section of a ZnO line passivated by a protective layer. When a mechanical stress is applied, a charge separation takes place. c) Cross section of a Au line and P(VDF-TrFE) film is deposited on top. When applying a mechanical stress, the P(VDF-TrFE) material creates a piezoelectric potential read out by the biased Au lines. d) Finite-element simulation of an ASL nanowall after applying a mechanical force on top of the structure. e) Schematic representation of a piezoelectric ZnO line terminated on both sides with Cr/Au electrodes. Below, the electronic band diagrams along the line structure are presented. Down-bending happens when applying a positive force and a negative current peak is generated. When a negative force is applied, an up-bending occurs and a positive current peak is generated.

(Figure 3d). The pulse potential appears locally while the rest of material remains neutral. The negative potential is induced under the point force which can be observed in the cross section in both the *x* and *y* directions. With this compressive force (negative sign) a negative field will be induced (vice versa) which means the induced potential and current will start with negative following by positive. The conduction mechanism of this device is demonstrated in Figure 3e. The piezoelectric line is very long compared to thickness and width. The pulse of negative potential lifts the local energy band structure upwards and the pulse of positive potential pulls the local band energy structure downwards. Due to the inequality of the generated potential along the piezoelectric material, a current is generated with respect to the potential pulse. A slight external bias potential on both electrode contacts can be applied to enhance the output piezoelectric current. This physical concept is suitable for the analysis of all three, the ASL, PSL and P(VDF-TrFE), force sensors because each of them shares the same 2D symmetry.

The signals of our respective piezoelectric force sensors were now measured and are shown in **Figure 4**. Figure 4a, c and e exhibit the output signals of single force-sensor lines based on PSL, ASL, and P(VDF-TrFE) principles, respectively. The applied forces in the μN range yield signals in the range of nA. Although the signal from each piezo force sensor is small, it is measurable which means it can be amplified in a commercially used version. Apparently, the more applied force, the more signal is generated. Comparatively, the ASL sensor provides the highest signal among the three sensors at a force of around 20 μN. This was expected because the cross-sectional area of the ASL-based ZnO line sensors was larger than the ones of the PSL sensors. However, the force-signal relation of the ASL sensors (Figure 4d) was not as good as PSL sensors (Figure 4b). The force-signal relation of the ASL sensors is non-linear, which leads to a force-signal saturation (Figure 4d), which means eventually the ASL force sensors will not react with the additional force correspondingly. However, for the PSL sensors, force signal saturation was not observed in our experiment (Figure 4b). Overall the piezoelectric effect in the ASL structure is much smaller due to the extreme wall geometry. With a thickness of 1 μm from the bottom to the top of the wall, the unipolarity of ZnO is destroyed; therefore the wall-like structure is not a good force sensor considerably. Compared with ASL sensors, PSL sensors provide a linear relation of force signal response which is very useful in terms of signal analysis. For example, the position between 2 lines can be anticipated just by the signal ratio of two lines. For the P(VDF-TrFE) sensor, the force response is different in terms of polarity. In every applied force, the signal response starts from positive current which is opposite to the signal response from ZnO. This is due to the fact that P(VDF-TrFE) has a negative piezoelectric constant d_{33}. The force-signal responses were observed as a linear relation, too, as seen in Figure 4f. Because the polymer conductivity is low, the generated current trapped by the Au electrode is limited, although the piezoelectric volume is much bigger.

The obtained device could be applied for potential detection of particles or biological species (e.g., cells or viruses) on a substrate. Although by this method directly it is still impossible to detect the weight of the biological DNA or cell, which can be in the range of 10^{-24}–10^{-12} kg, the cell or DNA might be positioned by a tip which yields enough force and electrical signal on the touchpad. The electrical information about the exact position of the cell by the tip can be stored and used for later investigations of the species at this particular position. While approaching a single particle or cluster to a position of the force detector, the

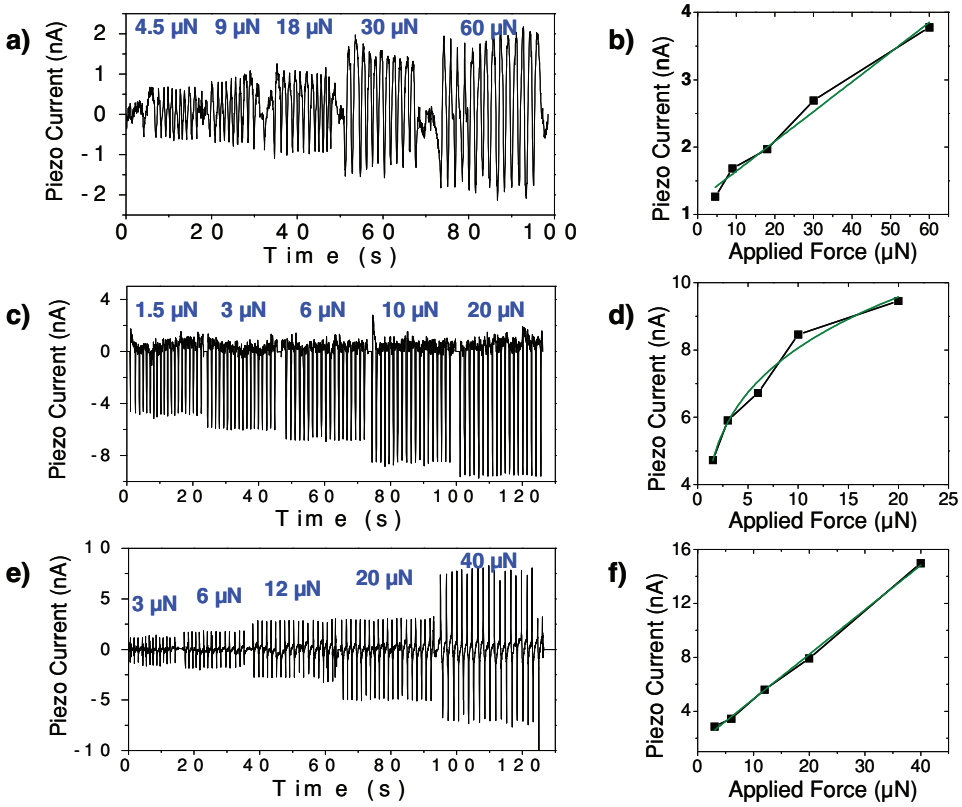

Figure 4. a,c,e) Time-resolved piezoelectric current responses of the PSL and ASL nanolines and the P(VDF-TrFE) sensor, respectively, when applying mechanical forces in the µN range. b,d,f) The respective piezoelectric peak-to-peak currents as a response to the applied mechanical forces. PSL (b) and P(VDF-TrFE) (f) representations show linear behavior while ASL (d) shows saturation effects due to the large volume of the structure.

position of the particle can be obtained while detecting the generated piezoelectric signal.

3. Conclusions

In conclusion, three types of large-scale high-resolution piezoelectric nano force position detectors so called PSL, ASL, and P(VDF-TrFE) sensors were fabricated and investigated. The PSL sensor combines a reliable signal with a simple fabrication process. Although the ASL sensor has a lower piezoelectric performance the resolution of the respective force-sensor array can be increased, because in the fabrication processes the dimension of the ASL lines can be scaled down much more. The P(VDF-TrFE) sensors have the simplest fabrication process with an optimum signal response. It also might be suitable for applications in flexible electronics because of the used polymer. All three types of force sensor can be fabricated as extremely high resolution force-sensor arrays which can define the position of an applied force very accurately. With the combination of the advanced lithography techniques presented here with nano piezoelectric effects, a superior high-resolution position detector for scientific use for instance as position markers for cells, DNA, nanotubes, and nanowires might be possible in the near future.

4. Experimental Section

Electromechanical Characterization: The electrical metal connections of the tested device were done by wire bonding to a carrier substrate containing electrical contacts for electrical measurements. Electrical measurements were realized using a Keithley 2636 source meter. For time-resolved measurements, the source meter was connected by GPIB to an external computer and read-out by a LabView program. For applying the mechanical force, a Honeywell force sensor FSS1500NST connected to a Wheatstone bridge including an instrumentation amplifier was used. The force sensor was attached to the microstage for a precise movement. Once the microstage touched the sample, the excessive force was read out by the sensor. The force value was collected corresponding to the electrical signal obtained from the piezoelectric platform.

Simulations: A COMSOL finite-element (FEM) simulation was used for the numerical calculations. We used strain-charge coupled equations and have implemented the piezoelectric properties of ZnO for constructive piezoelectric calculations. For demonstrating the effect of piezoelectric generation, the example of the fabricated PSL (phase-shift-lithography-based) device, which is presented in this paper, was simulated. A geometry exhibiting a height of 100 nm and a width of 300 nm was taken into account and an external stimulated point force of 1 µN was applied (similar to the applied range during the electromechanical characterization) onto the center on top of the wall. As a result the electrical potential was calculated. The pulse potential appeared locally, while the rest of the material remained neutral.

X-Ray Diffraction: The crystal structure was characterized by XRD θ–2θ scans using a Philips X'Pert MRD diffractometer with Cu Kα radiation.

Supporting Information

Supporting Information is available from the Wiley Online Library or from the author.

Acknowledgements

K.S. and A.M. contributed equally to this work. The authors thank Nikolai Zakharov and Peter Werner for the TEM measurements. This work was supported by Deutsche Forschungsgemeinschaft (DFG) under Contracts Za 191/24-1 and ZA 191/28-1.

Received: May 1, 2012
Revised: July 5, 2012
Published online: August 22, 2012

[1] W. Mohr, *US Patent* 3984738, **1974**.
[2] Z. Wu, X. Q. Bao, V. K. Varadan, V. V. Varadan, *Smart Mater. Struct.* **1992**, *1*, 330–340.
[3] A. Cricenti, R. Generosi, *Rev. Sci. Instrum.* **1995**, *66*, 2843–2847.
[4] A. Ruíz, A. Ramos, J. L. San Emeterio, *Ultrasonics* **2004**, *42*, 459–463.
[5] M. Taya, A. A. Almajid, M. Dunn, H. Takahashi, *Sens. Actuators A* **2003**, *107*, 248–260.
[6] S. Xu, Y. Qin, C. Xu, Y. Wei, R. Yang, Z. L. Wang, *Nat. Nanotechnol.* **2010**, *5*, 366–373.
[7] C. J. Hu, Y. H. Lin, C. W. Tang, M. Y. Tsai, W. K. Hsu, H. F. Kuo, *Adv. Mater.* **2011**, *23*, 2941–2945.
[8] J.-M. Kim, T. Nam, S. J. Lim, Y. G. Seol, N.-E. Lee, D. Kim, H. Kim, *Appl. Phys. Lett.* **2011**, *98*, 142113.
[9] Q. J. Wang, C. Pflügl, W. F. Andress, D. Ham, F. Capasso, M. Yamanishi, *J. Vac. Sci. Technol. B* **2008**, *26*, 1848–1851.
[10] J. Du, Z. Cui, X. Yuan, Y Guo, *Microelectron. Eng.* **2002**, *61*, 265–27.
[11] K. Subannajui, F. Güder, M. Zacharias, *Nano Lett.* **2011**, *11*, 3513–3518.
[12] F. Güder, Y. Yang, M. Krüger, G. B. Stevens, M. Zacharias, *ACS Appl. Mater. Interfaces* **2010**, *2*, 3473–3478.
[13] Y.-K. Choi, J. Zhu, J. Grunes, J. Bokor, G. A. Somorjai, *J. Phys. Chem. B* **2003**, *107*, 3340–3343.
[14] H.-W. Ra, K.-S. Choi, J.-H. Kim, Y.-B. Hahn, Y.-H. Im, *Small* **2008**, *4*, 1105–1110.
[15] S. Bauer, F. Bauer, in *Piezoelectricity*, (Eds: W. Heywang, K. Lubitz, W. Wersing), *Springer Series in Materials Science, Vol. 114*, Springer, Berlin **2008**, 157–177.
[16] A. V. Bune, C. Zhu, S. Ducharme, L. M. Blinov, V. M. Fridkin, S. P. Palto, N. G. Petukhova, S. G. Yudin, *J. Appl. Phys.* **1999**, *85*, 7869–7873.
[17] F. Güder, Y. Yang, S. Goetze, A. Berger, R. Scholz, D. Hiller, D. Hesse, M. Zacharias, *Chem. Mater.* **2011**, *23*, 4445–4451.
[18] D. Damjanovic, *Rep. Prog. Phys.* **1998**, *61*, 1267–1324.
[19] G. R. Fox, D. Damjanovic, P. A. Danai, N. Setter, H. G. Limberger, N. H. Ky, *Mater. Res. Soc. Symp. Proc.* **1994**, *360*, 389–394.
[20] J. Y. Kim, S.-H. Ko Park, H. Y. Jeong, C. Park, S.-Y. Choi, J.-Y. Choi, S.-H. Han, T. H. Yoon, *Bull. Korean Chem. Soc.* **2008**, *29*, 727–728.
[21] I. K. Bdikin, J. Gracio, R. Ayouchi, R. Schwarz, A. L. Kholkin, *Nanotechnology* **2010**, *21*, 235703.